applied sciences

MDPI

Article

An Adaptive Maximum Power Point Tracker for Photovoltaic Arrays Using an Improved Soft Computing Algorithm

Kuei-Hsiang Chao * and Shu-Wei Zhang

Department of Electrical Engineering, National Chin-Yi University of Technology, Taichung 41170, Taiwan; zhangshuwei0617@gmail.com

* Correspondence: chaokh@ncut.edu.tw; Tel.: +886-4-2392-4505 (ext. 7272); Fax: +886-4-2392-2156

Abstract: This paper presents an improved version of the firefly algorithm (FA) by which a maximum power point (MPP) tracker was developed to track down the global maximum power point (GMPP) of a partially shaded photovoltaic module array (PVMA). As the first step, our team developed a high-voltage step-up converter where a coupled inductor was used to store the energy so that the duty cycle can be reduced so as to raise the voltage gain. The single-peaked P-V output characteristic curve of a PV array turns out to contain multiple peaks when the array is partially shaded. As a consequence, conventional MPP trackers occasionally track down a local maximum power point (LMPP), instead of the desired GMPP, and the output power of the array falls accordingly. Therefore, an improved version of the FA is proposed as a way to ensure that the GMPP can be tracked down in a more efficient way. Using the Matlab software, the MPP tracking performance of the proposed tracker was finally simulated in five scenarios. As it turned out, the proposed converter provided a high voltage gain at a relatively low duty cycle, and the improved version of the FA outperformed the original in terms of tracking time.

Keywords: firefly algorithm; partially shaded; photovoltaic module array; maximum power point tracker; high-voltage step-up converter; coupled inductor; local maximum power point; global maximum power point

Citation: Chao, K.-H.; Zhang, S.-W. An Adaptive Maximum Power Point Tracker for Photovoltaic Arrays Using an Improved Soft Computing Algorithm. *Appl. Sci.* **2023**, *13*, 6952. https://doi.org/10.3390/app13126952

Academic Editors: Manuela Sechilariu, Saleh Cheikh-Mohamad and Berk Celik

Received: 26 April 2023
Revised: 31 May 2023
Accepted: 5 June 2023
Published: 8 June 2023

1. Introduction

Solar power has been acknowledged as one of the most promising renewable energy sources, particularly in places with long hours of sunshine [1,2]. A maximum power point tracker is employed to increase the power generation efficiency of a solar energy system. The perturbation and observation (P&O) [3–8] algorithm and the incremental conductance (INC) algorithm [9–11] are two of the commonest algorithms to track the MPP on a P-V curve of a PV array. However, these two algorithms occasionally do not track down the GMPP of a shaded PV array as expected. Instead, they get trapped in an LMPP.

Over the years, there has been a multitude of publications on tracking the MPP of a shaded PV array in the literature. Here are a number of frequently used algorithms on this issue: fuzzy logic control algorithms [12–14], neural networks (NN) [15–17], the grey wolf optimization (GWO) algorithm [18–20], the differential evolution (DE) algorithm [21–23], the artificial bee colony (ABC) algorithm [24–26], the firefly algorithm (FA) [27–30], the variable step size perturbation and observation (P&O) [31] and the shuffled frog-leaping (SFL) algorithm [32]. In the fuzzy control algorithms [12–14], input data are converted into fuzzy data, a membership function is used to map the fuzzy data into member attributes. Then, the attributes are expressed as a sequence of if–then rules for subsequent fuzzy operations. Finally, the fuzzy data are converted back to the non-fuzzy data as output. Consequently, fuzzy algorithms require a large amount of time to perform complex operations, that is, a high time complexity. NNs such as those in [15–17] mimic the way that biological neurons signal to one another and have been used to simplify information processing in complicated nonlinear models and particularly well applied to artificial intelligence (AI) and deep

learning recently. However, a pyrometer and an exact fill factor [33] are required when an NN is applied to deal with the MPP tracking issue. As a consequence, the hardware cost is raised, and the MPP tracking accuracy remains an issue as well. In [18–20], the GWO algorithm mimics the social hierarchy and the hunting mechanism of grey wolves in nature. In a pack of grey wolves, there are three hierarchies responsible for seeking, encircling and finally attacking prey, respectively, in order to optimize the hunting performance. Although the GWO algorithm is simple and requires a smaller number of parameters to run global optimization, its major disadvantages include poor tracking accuracy, slow convergence and particularly the likelihood of getting stuck in a local solution. The DE algorithm in [21–23] is essentially a heuristic model and works in a similar way to the genetic algorithm (GA). It performs real number coding on a specific population. The global optimum is sought by evaluating the variance and using the one-to-one competitive strategy for survival. However, a major disadvantage is that it requires more operations and consequently takes a longer period of time to perform a global search when there is a genetic mutation in an individual. However, inappropriate parameter setting frequently leads to over-speedy convergence. As a result, the DE algorithm gets trapped in a local maximum and fails to reach the global maximum. The ABC algorithm [24–26] is a global optimization algorithm that mimics the intelligent foraging behavior of honeybees in nature. Employed bees search for food sources. As it turns out, the ABC algorithm provides high stability and requires a smaller number of parameters, while suffering the disadvantage of over-speedy convergence as the GA does. Proposed by Xin-She Yang in 2008, the FA [27–30] mimics the flashing behavior of fireflies. In nature, fireflies are attracted to each other by blinking signals. The more brightly a firefly glows, the more fireflies it attracts. Particularly, fireflies are randomly attracted to different light sources with the same intensity. Consequently, the brightest firefly is the optimal solution. The FA requires a smaller number of parameters and provides a wide search scope, fast convergence and high stability, while being very likely to get trapped in a local optimum solution, particularly in a multi-dimensional problem. The variable step size P&O method [31] is considerably sensitive to the initial parameter values, so the performance of its maximum power tracking controller is highly dependent on the selection of initial parameters. Therefore, the parameters must be selected and controlled carefully for this tracking technology, or there would be a significant impact on the tracking performance of its algorithm. Moreover, it is necessary to pay attention to the selection of the sample distribution and the adjustment of the parameters in order to improve the performance of the algorithm and increase the convergence speed. As for the shuffled frog-leaping (SFL) algorithm [32], a large amount of storage space and computing resources are usually required, and the increase in the number of groups will slow down the execution of the algorithm. Even more, insufficient computer memory capacity might be a result. Moreover, more parameters need adjustment while different parameters might need to be used in different application scenarios. Therefore, it becomes more difficult to adjust the parameters of the algorithm.

In light of this, this paper presents an improved version of the FA to locate the GMPP of a P-V curve with multiple peaks. The improved version is simple and straightforward; the step size in particular is made adaptive to the slope of a P-V characteristic curve. In this manner, it takes the improved version a shorter period of time to get away from a LMPP than the original, and the GMPP can be tracked down more efficiently.

Due to advances in power electronics, converters have been widely applied to MPP trackers so as to raise the power generation efficiency of a PV array. However, a major disadvantage of conventional DC-DC converters is the low voltage ratio due to the typical duty cycle [34–36]. For this sake, a great amount of effort has been put over the years into developing converters with a high voltage ratio. For example, the voltage ratio was raised as intended using coupled inductors with a high turn ratio [37–40]. Nonetheless, this move increased the output ripple voltage of a converter. Based on the same configuration as in [37–40], a converter is presented in this work as a solution to the above-referred problem. Inductors were replaced with coupled inductors therein so as to raise the voltage ratio,

and clamp capacitors were also used to suppress the output voltage ripples in an effort to improve the performance of the converter. The presented converter was then simulated using PSIM software [41] for performance validation.

The organization of this paper is arranged as follows. The working principle of the adopted high boost ratio converter and its component design are described herein in Section 2. Next, the P-V and I-V output characteristics of a PV module under shading are described in Section 3. Subsequently, the working principle of the conventional FA is described, followed by proposing an improved FA, in Section 4. Finally, some simulation tests are performed in Section 5 to verify the effectiveness of the proposed improved FA for MPPT.

2. High Voltage Boost Converter

The adopted high-voltage boost converter is illustrated in Figure 1 [42]. The rated input and output voltages of the converter are 80 and 400 V, respectively.

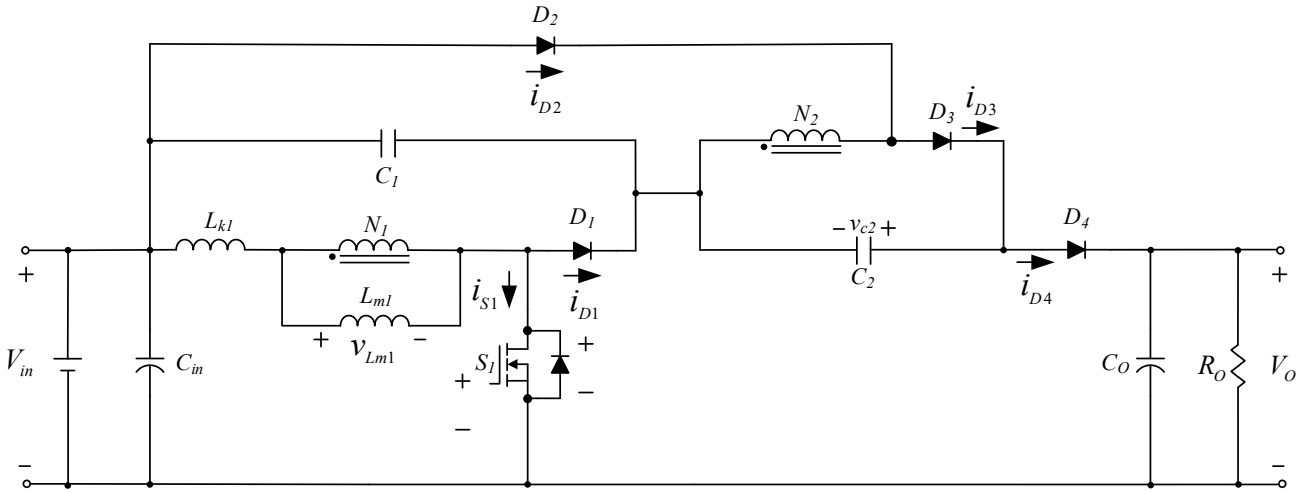

Figure 1. The presented high-voltage step-up converter.

For simplicity, the voltage drops across each forward-biased diode; the main switch S_1 when remaining on and the inductor L_{k1} are all neglected. The duty cycle D is defined as

$$D \triangleq \frac{t_{on}}{T} \tag{1}$$

where t_{on} represents the period of time that S_1 remains on, and T is the operation period of the converter.

(1) Mode 1 ($t_0 \sim t_1$)

The circuit conduction situation in this mode is indicated in Figure 2. S_1 remains on, and the input voltage V_{in} is directly applied to the primary side N_1 of the coupled inductor. Accordingly, the current through the secondary side N_2 charges the capacitor C_1, and the diode D_2 remains forward-biased until S_1 is turned off at the end of this mode. The voltage drops across components and the currents therethrough are governed by

$$\Delta i_{Lm1(closed)} = \frac{V_{in}}{L_{m1}} DT \tag{2}$$

$$v_{N2} = v_{C1} = V_{in} \frac{N_2}{N_1} \tag{3}$$

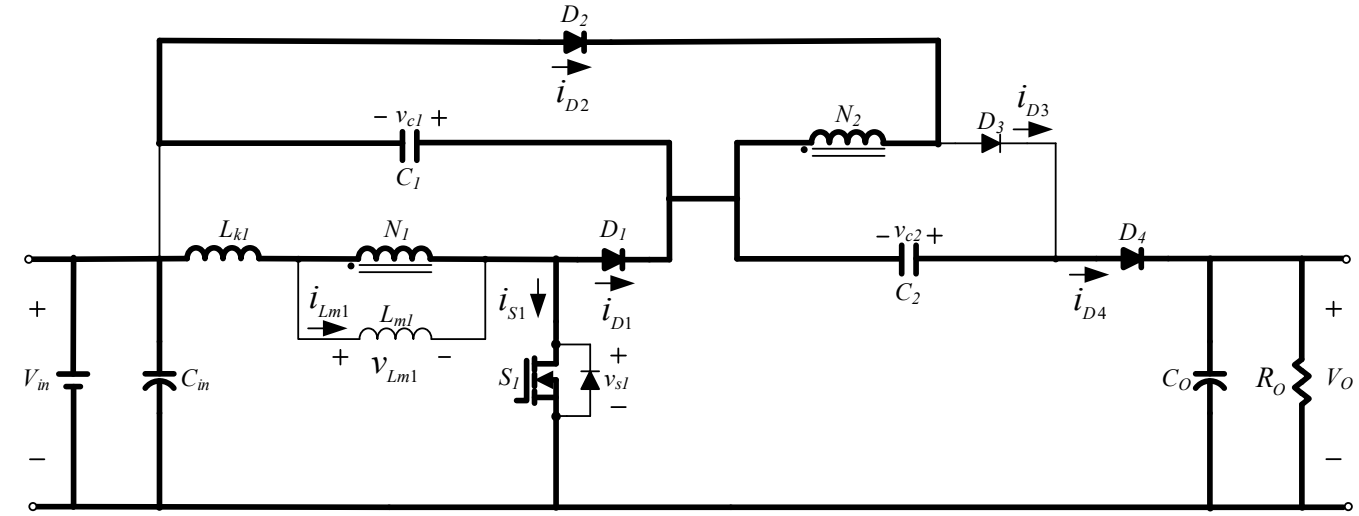

Figure 2. Circuit conduction situation in Mode 1.

(2) Mode 2 ($t_1 \sim t_2$)

The circuit conduction situation in this mode is indicated in Figure 3. S_1 is switched off, and D_1 is forward-biased. The energy stored in N_1 is released to C_1, and the polarity of N_2 is reversed. As a consequence, the diode D_3 is forward-biased, and the capacitor C_2 is charged until the energy stored in N_1 is completely released. The governing equation is expressed as

$$v_{N1} = v_{Lm1} = v_{N2}\frac{N_1}{N_2} = v_{C2}\frac{N_1}{N_2} \tag{4}$$

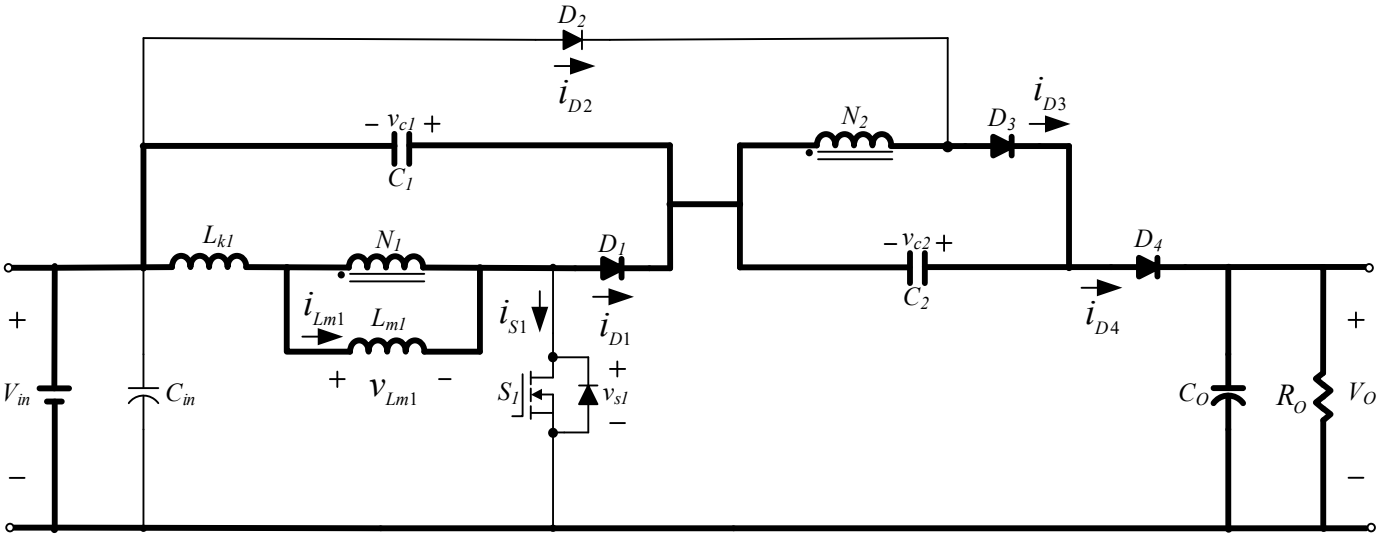

Figure 3. Circuit conduction situation in Mode 2.

(3) Mode 3 ($t_2 \sim t_3$)

The circuit conduction situation in this mode is indicated in Figure 4. S_1 remains off. The energy stored in C_1, C_2 and L_{m1} is released to the load by way of the diode D_4, and an operation cycle is completed accordingly.

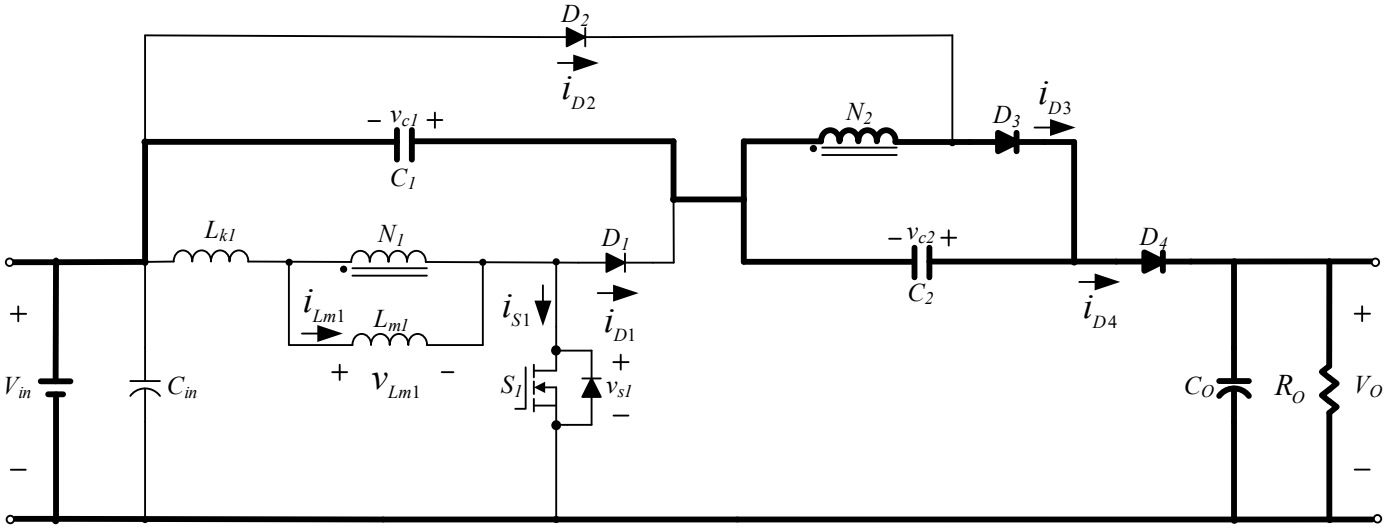

Figure 4. Circuit conduction situation in Mode 3.

The inductor volt-second balance theory states that, in the steady state, the net change in the current flowing through an inductor is zero over a cycle. Therefore, applying the principle to Equations (2) and (4) gives

$$V_{in}DT = \frac{N_1}{N_2} v_{C2}(1-D)T \tag{5}$$

Rearranging Equation (5) gives

$$v_{C2} = \frac{N_2}{N_1} V_{in} \frac{D}{1-D} = \frac{ND}{1-D} V_{in} \tag{6}$$

The output voltage is given by

$$V_o = V_{in} + v_{C1} + v_{C2} \tag{7}$$

Substituting Equations (3) and (6) into Equation (7) gives the voltage ratio

$$\frac{V_o}{V_{in}} = \frac{N_1 + N_2}{N_1} + \frac{N_2}{N_1} \frac{D}{1-D} = \frac{1+N-D}{1-D} \tag{8}$$

Assuming that all the components are lossless, the input power is equal to the output power, i.e., $P_{in} = P_{out}$, and

$$V_{in} I_{Lm1} = \frac{{V_o}^2}{R} \tag{9}$$

Substituting Equations (8) and (9) into Equation (7) gives

$$I_{Lm1} = \frac{{V_o}^2}{V_{in} R} = \frac{{V_o}^2}{{V_{in}}^2} \frac{V_{in}}{R} = \left(\frac{1+N-D}{1-D}\right)^2 \frac{V_{in}}{R} \tag{10}$$

where $(\frac{1+N-D}{1-D})$ is the voltage ratio of the converter.

Derived from Equation (2), the increment of i_{Lm1}, over the period of time DT that S_1 is on, is given by

$$\Delta i_{Lm1(closed)} = \frac{V_{in}}{L_{m1}} DT \tag{11}$$

Accordingly, the maximum and the minimum magnetizing current of the inductor, $I_{Lm1(\max)}$ and $I_{Lm1(\min)}$, are respectively given by

$$I_{Lm1(\max)} = I_{Lm1} + \frac{\Delta i_{Lm1}}{2} = V_{in}\left[\left(\frac{1+N-D}{1-D}\right)^2 \frac{1}{R} + \frac{D}{2L_{m1}f}\right] \tag{12}$$

$$I_{Lm1(\min)} = I_{Lm1} - \frac{\Delta i_{Lm1}}{2} = V_{in}\left[\left(\frac{1+N-D}{1-D}\right)^2 \frac{1}{R} - \frac{D}{2L_{m1}f}\right] \tag{13}$$

The inductor current is continuous on the condition that $I_{Lm1(\min)} \geq 0$, that is,

$$L_{m1(\min)} \geq \frac{D}{2f}\frac{(1-D)^2 R}{(1+N-D)^2} \tag{14}$$

The rated output power and the output voltage are specified as 300 W and 400 V, respectively, in Table 1, and the load R_O is evaluated as 533.33 Ω accordingly. It is requested that the inductor L_{m1} works anytime in the continuous conduction mode (CCM), that is, $I_{Lm1(\min)} \geq 0$ anytime, regardless of any change in the solar irradiance. As illustrated in Figure 5, the peak of the curve $y = \frac{D(1-D)^2}{(1+2-D)^2}$ occurs at $D = 0.394$. Substituting $D = 0.394$, $R_O = 533.33\ \Omega$, $f = 25$ kHz and the turn ratio $N = 2$ into Equation (14) gives $L_{m1} = 227\ \mu$H. However, L_{m1} is multiplied by a factor of 1.25, that is, L_{m1} is raised from 227 to 284 μH, to ensure that the converter works all the time in the CCM as expected. Since V_{c1} is evaluated as 160 V in Equation (3), a 2 μF/250 V film capacitor is used as C_1. The maximum duty cycle of S_1 is specified as 0.75. Substituting $D = 0.75$ into Equation (6) gives $V_{c2} = 480$ V, and a 5 μF/630 V film capacitor is used as C_2 accordingly.

Table 1. Specifications of the presented converter.

Input voltage (V_{in})	80 V
Output voltage (V_O)	400 V
Output power (P_O)	300 W
Switching frequency of power switch (f)	25 kHz
Turn ratio of inductor ($N = N_2/N_1$)	2

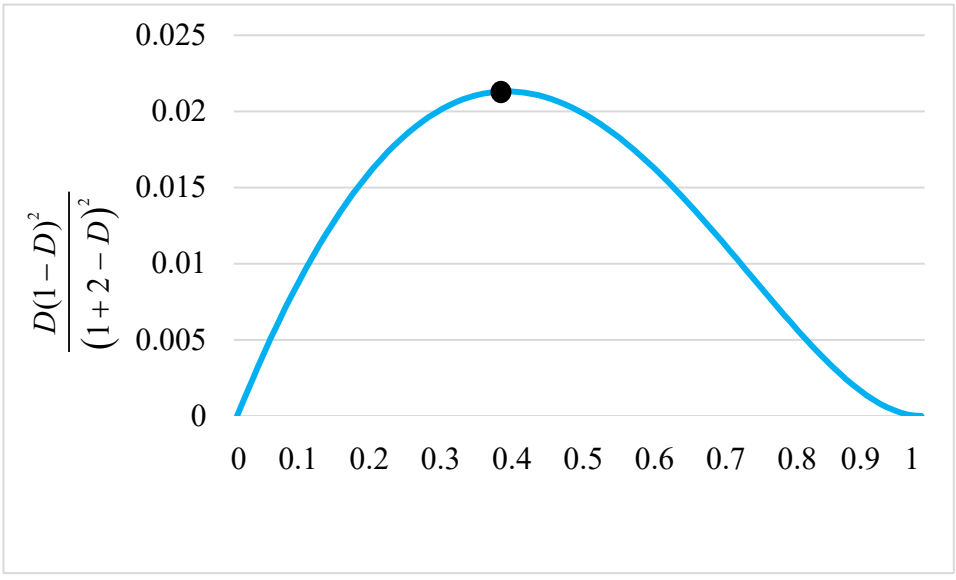

Figure 5. A graph of $\frac{D(1-D)^2}{(1+2-D)^2}$ against D.

3. Shading Dependence of Output Characteristics of a PV Array

A single-peaked P-V characteristic curve of a PV array happens to contain multiple peaks if the array is partially shaded in different series and parallel combinations. In this work, SW20W PV modules, manufactured by MPPTSUN Co. Ltd., China, were used to build a PV array under test. Specifications of an SWM20W PV module are listed in Table 2. Using the Matlab software, a family of I-V and P-V characteristic curves of a 4 series-3 parallel (4S-3P) PV array, as shown in Figure 6, were simulated under Standard Test Conditions (STCs), that is, with the solar irradiance = 1 kW/m^2, T = 25 °C and air mass (AM) = 1.5. As illustrated in Figure 7, the improved version of the firefly algorithm was applied to track down the GMPP of a P-V array by controlling the gate of the main switch in the converter.

Table 2. Specifications of an SWM20W PV module.

Parameter	Specification
Maximum output power (P_{max})	20 W
Current of MPP (I_{mpp})	1.10 A
Voltage of MPP (V_{mpp})	18.18 V
Short current (I_{sc})	1.15 A
Open voltage (V_{oc})	22.32 V
Size of module	395 × 345 × 17 mm

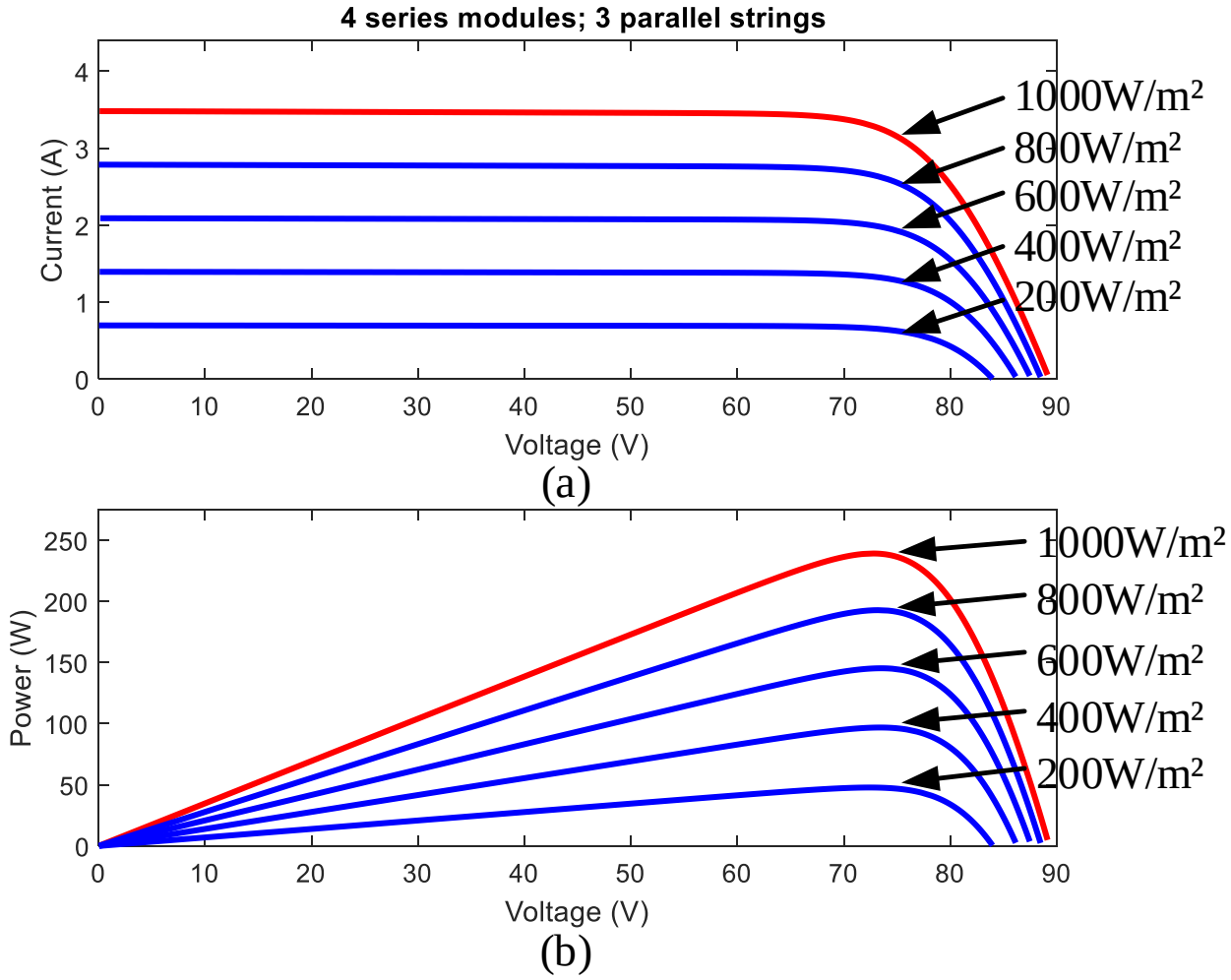

Figure 6. A family of (**a**) I-V and (**b**) P-V curves for a 4S-3P configuration with shading as a parameter.

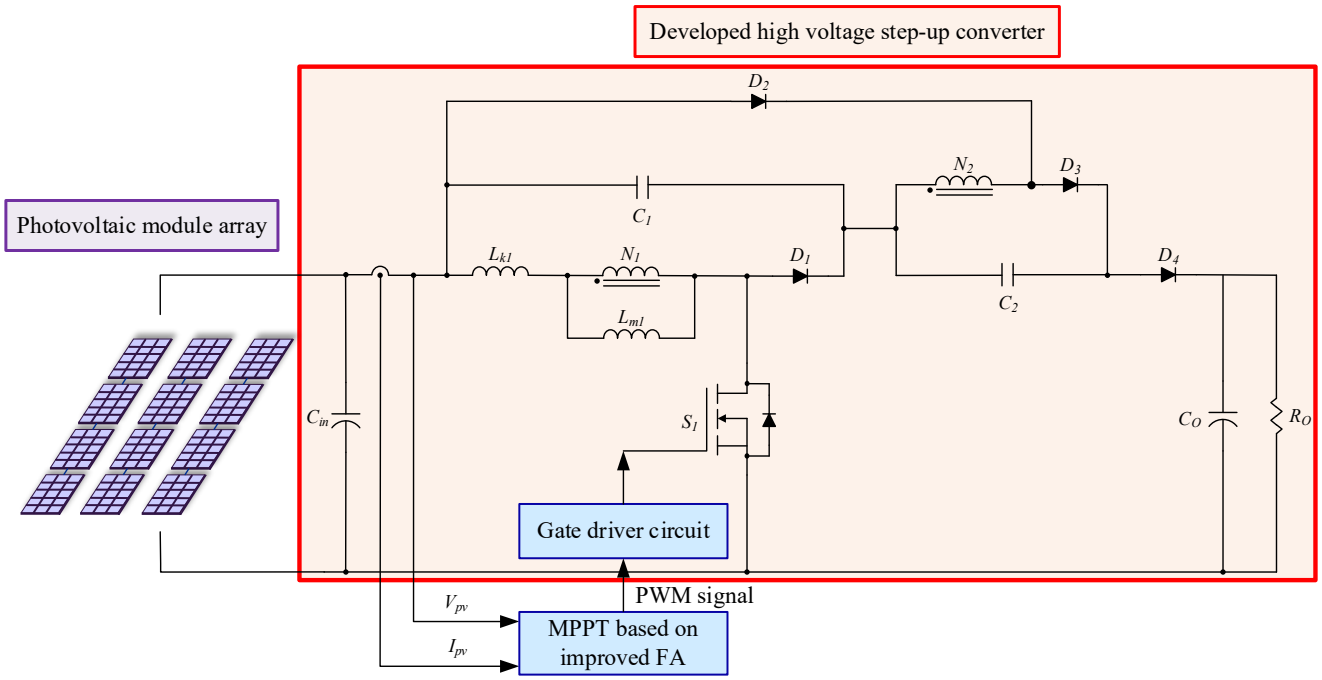

Figure 7. Framework of the presented MPP tracker.

4. Firefly Algorithms

As referenced previously, the FA is actually a heuristic model proposed by Xin-She Yang in 2008. Fireflies communicate to each other by blinking signals. In nature, fireflies emitting flashes of light weakly are attracted to those emitting strongly, while moving randomly between two light sources with the same intensity. The more a firefly glows, the better a position it has. Accordingly, the firefly which glows most is the optimal solution. Compared to other algorithms, the FA requires a smaller number of parameters, has a wide search scope and provides high stability. However, with a poor starting point for a search or a poor choice of a step size, the FA would fail to track down the global optimum, especially in a multi-dimensional problem. Instead, it could get trapped in a local optimum.

4.1. The Conventional FA

The FA works under the following assumptions.

(1) Fireflies are attracted to each other despite their gender.
(2) Level of attraction is simply a function of the light intensity and the distance between fireflies, and it decreases as the distance increases. Fireflies which glow with lower brightness are attracted to those with higher brightness—which move randomly.

Here are the steps to find the optimum solution.

Step 1: Initialize the number of fireflies m, the maximum number of iterations $It_{\max}$ and the step size a.

Step 2: The relative brightness between a firefly and another is given by

$$\beta = \beta_0 e^{-\alpha d_{ji}^2} \tag{15}$$

where β_0 represents the brightness emitted by the firefly, and α the absorption coefficient of a medium. β_0 decays as the distance increases, and α is usually considered a constant.

Step 3: In an n-dimensional space, the distance between fireflies i and j is expressed as

$$d_{ji} = ||x_j - x_i|| = \left[\sum_{k=1}^{n}\left(x_{j,n} - x_{i,n}\right)^2\right]^{\frac{1}{2}} \tag{16}$$

where $x_{j,n}$ represents the n coordinate of firefly j. In this work, the FA is applied to track the MPP of a PV array, and the n-dimensional space is therefore simplified to a plane. Hence, Equation (16) becomes

$$d_{ji} = \left[\left(x_j - x_i\right)^2 + \left(y_j - y_i\right)^2\right]^{\frac{1}{2}} \tag{17}$$

Step 4: Level of attraction is given by

$$\gamma = \gamma_0 e^{-\alpha d_{ji}^2} \tag{18}$$

where γ_0 represents the maximum of γ.

Step 5: Firefly i is attracted to firefly j, and the position of firefly i is updated using

$$x_i^{it+1} = x_i^{it} + \gamma_0 e^{-\alpha d_{ji}^2}\left(x_j^{it} - x_i^{it}\right) + a r_i^{it} \tag{19}$$

where r is a random number between 0 and 1.

Step 6: Go back to Step 1 until the maximum number of iterations is reached, and then output x_i.

4.2. The Improved FA

Firstly, the upper and the lower bounds of a are specified, and a is updated using

$$a = (1 - \frac{it}{It_{max}})a_{max} + \frac{it}{It_{max}} \times a_{min} \tag{20}$$

where a_{max} and a_{min} represent the upper and the lower bound of a, respectively, and it represents the number of iterations. Subsequently, a is slightly tuned according to the slope s of a P-V curve, as illustrated in Figure 8. Table 3 lists the correlation between s and the slightly tuned a, and it must be stressed that a is tuned on the condition that $\Delta P > 0$. In this fashion, the GMPP can finally be tracked down. A flowchart combining the conventional FA and the improved FA in Figure 9 is used to illustrate the working steps of the conventional FA and the improved FA in this study.

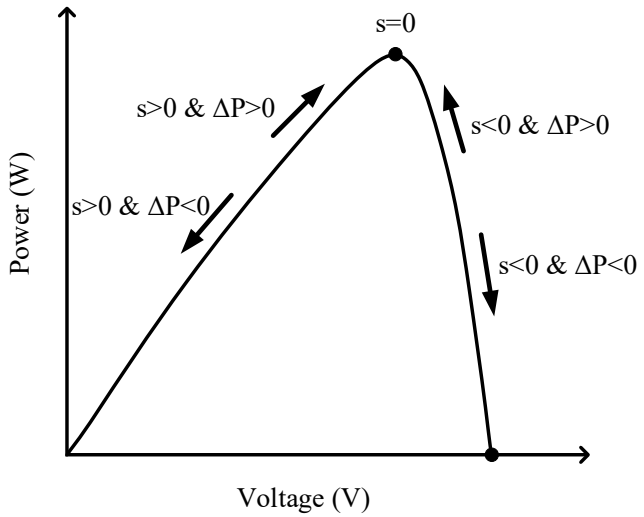

Figure 8. Illustration of the change in s and ΔP along a P-V curve.

Table 3. Correlation between s and the slightly tuned a.

$s \triangleq \frac{P_{(it+1)}-P_{(it)}}{V_{(it+1)}-V_{(it)}}$	**Fine-Tuning a of Equation (20)** $\left(\begin{array}{c}\Delta P = P_{(it+1)} - P_{(it)} \\ \Delta P > 0\end{array}\right)$
$s > 2$	a of Equation (20) + s × 0.01
$2 \geq s > 1.5$	a of Equation (20) + s × 0.01
$1.5 \geq s > 1$	a of Equation (20) − s × 0.01
$1 \geq s > 0.5$	a of Equation (20) − s × 0.03
$0.5 \geq s > 0$	a of Equation (20) − s × 0.04
$s = 0$	a
$0 > s \geq -0.5$	a of Equation (20) + s × 0.04
$-0.5 > s \geq -1$	a of Equation (20) + s × 0.03
$-1 > s \geq -1.5$	a of Equation (20) + s × 0.01
$-1.5 > s \geq -2$	a of Equation (20) − s × 0.01
$s < -2$	a of Equation (20) − s × 0.01

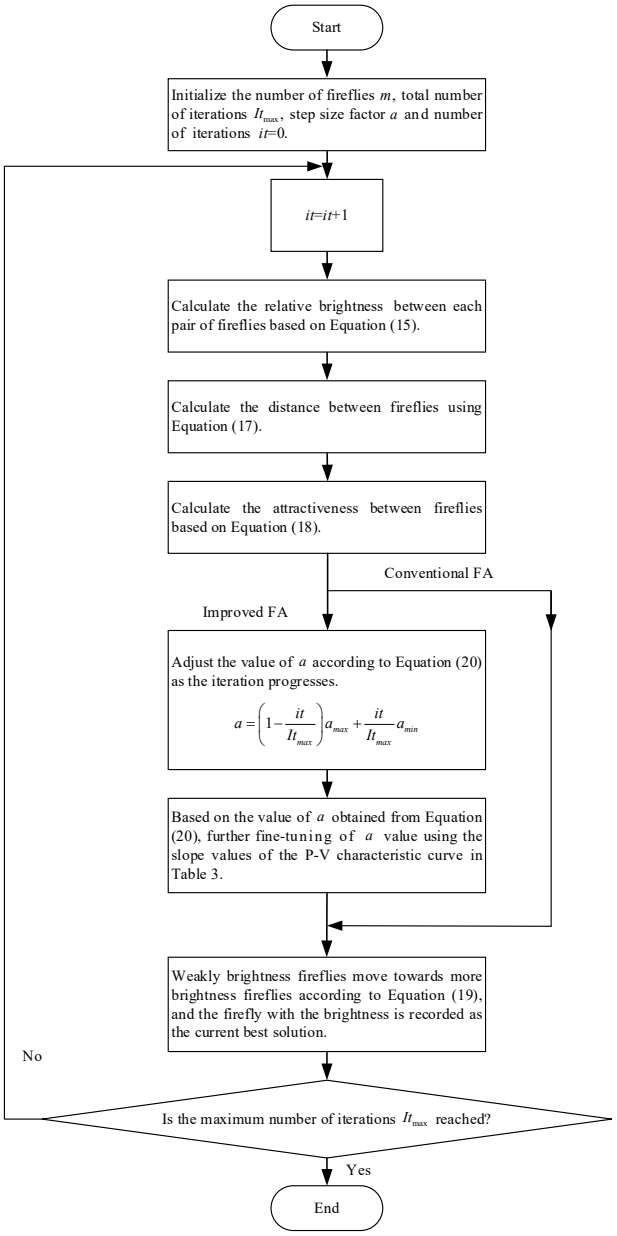

Figure 9. A flowchart combining the conventional FA and the improved FA.

5. Simulation Results

The proposed high-voltage step-up converter was simulated using the PSIM software, and MPPT was then simulated using the Matlab software.

5.1. Simulation Results of the Proposed Converter

Figure 10 gives waveforms of the simulated input voltage V_{in}, output voltage V_O and the duty cycle D signal at a full load of 300 W. An input voltage of 80 V was raised to an output voltage of 400 V when D was 0.567.

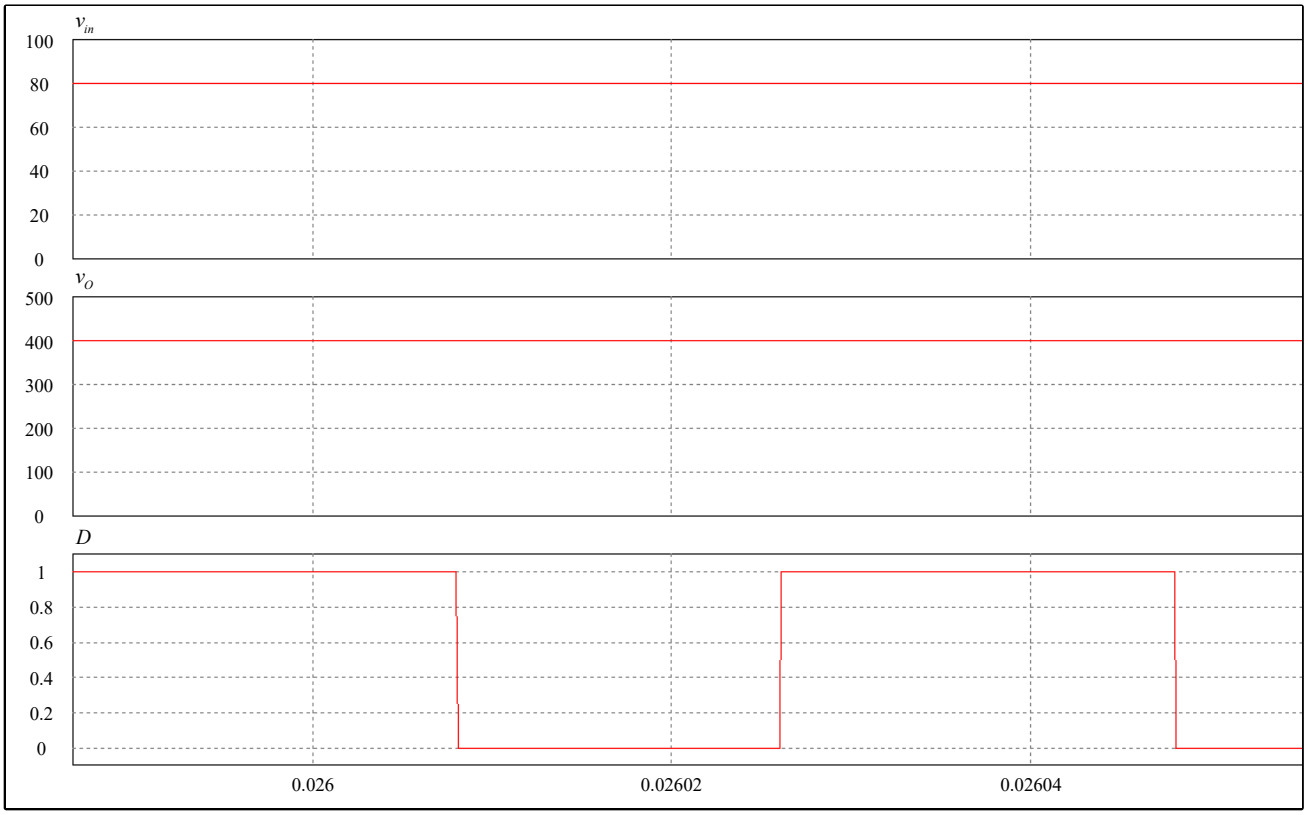

Figure 10. Waveforms of the simulated input voltage V_{in}, output voltage V_O and the gate drive signal at full load of 300 W.

5.2. Simulation Results of the Improved FA

Tables 4 and 5 list the parameter settings used in the conventional and the improved version of the firefly algorithm. Table 6 lists five scenarios, representing five different shading conditions, in which shading effects on P-V characteristic curves of a 4 series-3 parallel (4S-3P) configuration were demonstrated. As will be seen below, multiple peaks occurred in the P-V curves in Scenarios 2–5 where the GMPP lay near the left or right endpoint of the P-V curves. The GMPP tracking performance was simulated in each scenario and then compared to highlight the advantage of this work over others.

Table 4. Parameter settings in the original version of the FA.

Parameter Name	Value
Number of fireflies (m)	4
Maximum number of iterations (It_{max})	30
Step size (a)	2

Table 5. Parameter settings in the improved version of the FA.

Parameter Name	Value
Number of fireflies (m)	4
Maximum number of iterations (It_{max})	30
Upper bound of a step size ($a_{\max}$)	2.5
Lower bound of a step size ($a_{\min}$)	1.5

Table 6. Shading description of Scenarios 1–5.

Scenario	Module Connection and Shading Condition	Number of P-V Curve Peaks

1	(0% shading + 0% shading + 0% shading +0% shading)//
	(0% shading + 0% shading + 0% shading + 0% shading)//
	(0% shading + 0% shading + 0% shading +0% shading)
		Single

2	(0% shading + 0% shading + 0% shading + 50% shading)//
	(0% shading + 0% shading + 0% shading + 0% shading)//
	(0% shading + 0% shading + 0% shading + 0% shading)
		Double
		(MPP was on the rightmost peak)

3	(0% shading + 0% shading + 50% shading + 70%shading)//
	(0% shading + 0% shading + 0% shading + 0% shading)//
	(0% shading + 0% shading + 0% shading + 0% shading)
		Triple
		(MPP was on the rightmost peak)

4	(0% shading + 30% shading + 50% shading + 70% shading)//
	(0% shading + 0% shading + 0% shading + 0% shading)//
	(0% shading + 0% shading + 0% shading + 0% shading)
		Triple
		(MPP was on the rightmost peak)

5	(0% shading + 70% shading + 80% shading + 90% shading)// (0% shading + 70% shading + 80% shading + 90% shading)// (0% shading + 70% shading + 80% shading + 90% shading)	Quadruple (MPP was on the leftmost peak)

Note: "+" represents series and "//" represents parallel.

(1) Scenario 1

In this scenario, the PV array was unshaded and provided a maximum output power of 239.1 W, as illustrated in Figure 11. The tracking performance is compared in Figure 12. It can be easily seen that this work outperformed the original FA and the traditional P&O method.

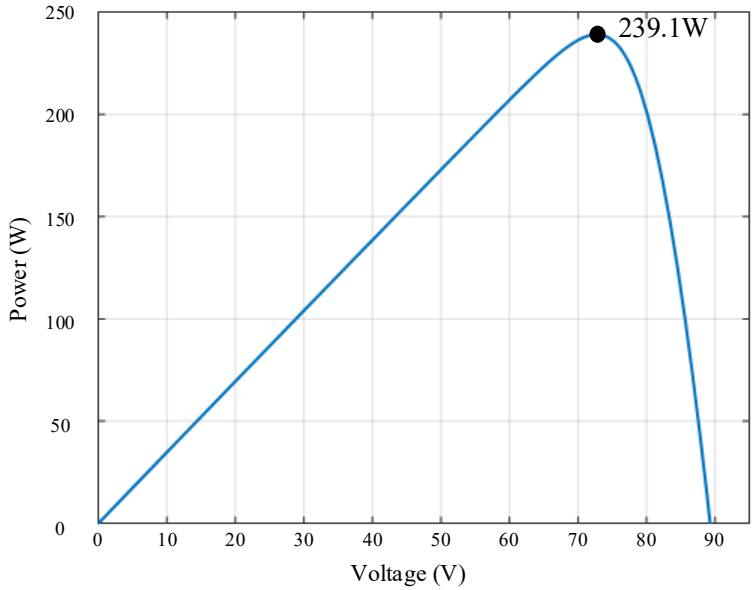

Figure 11. The P-V curve in Scenario 1.

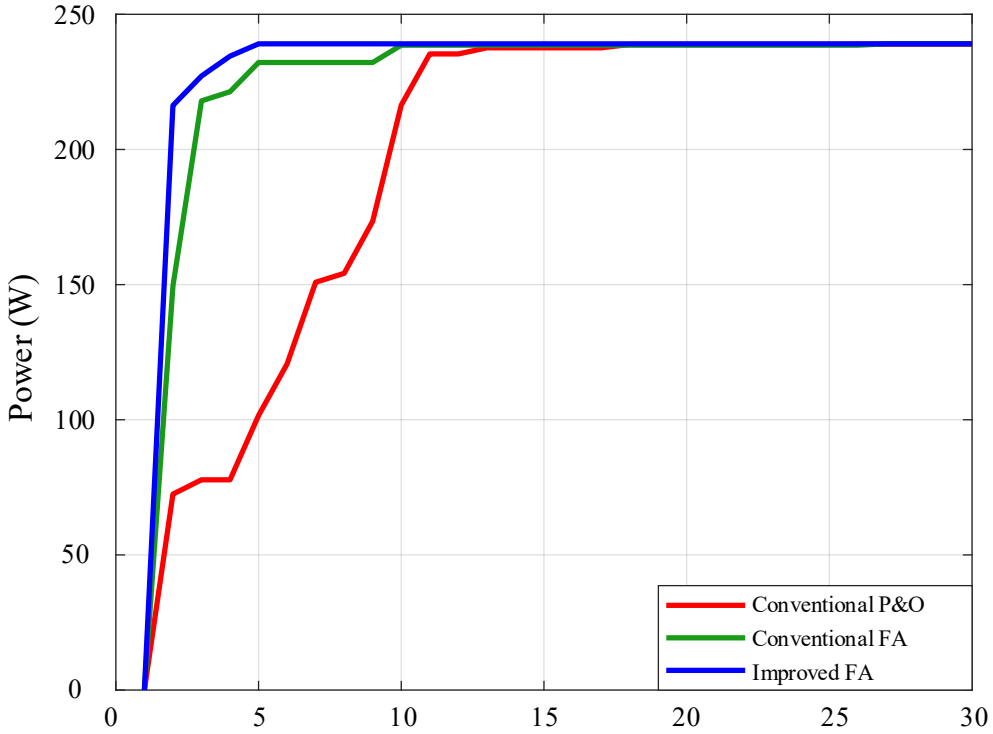

Figure 12. A tracking performance comparison between algorithms in Scenario 1.

(2) Scenario 2

In this scenario, 50% of a module was shaded. As illustrated in Figure 13, there were two peaks on the P-V curve, and the maximum power fell from 239.1 to 201.7 W. Similar to Scenario 1, the GMPP lay near the right endpoint of the curve. As can be seen in Figure 14, the GMPP can be tracked down well using any of the three approaches, and it is noted that this work outperformed others again.

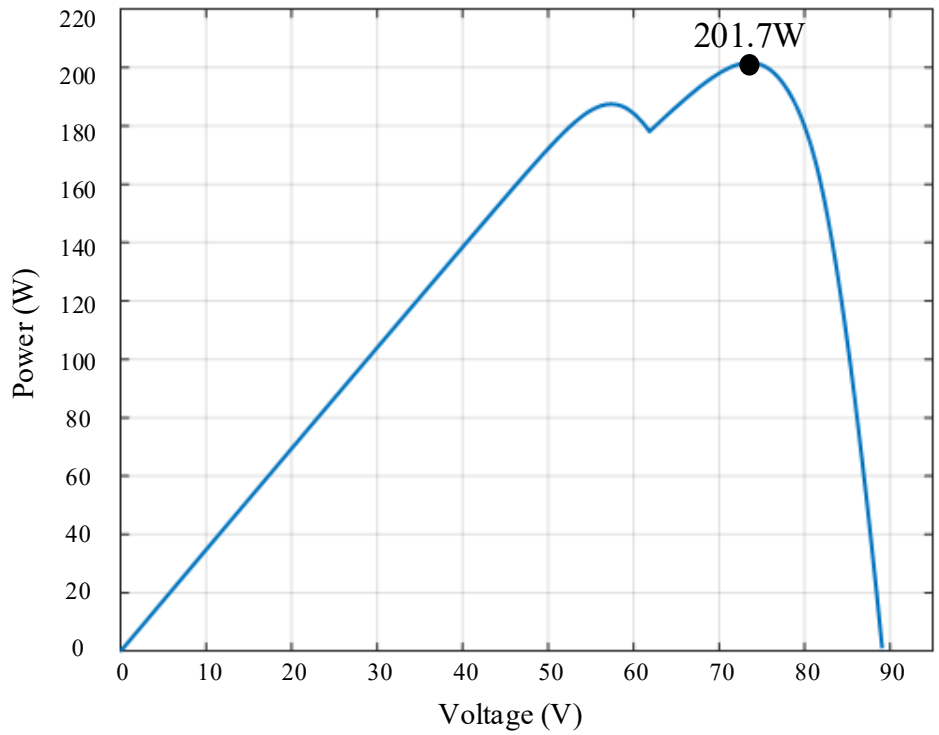

Figure 13. The P-V curve in Scenario 2.

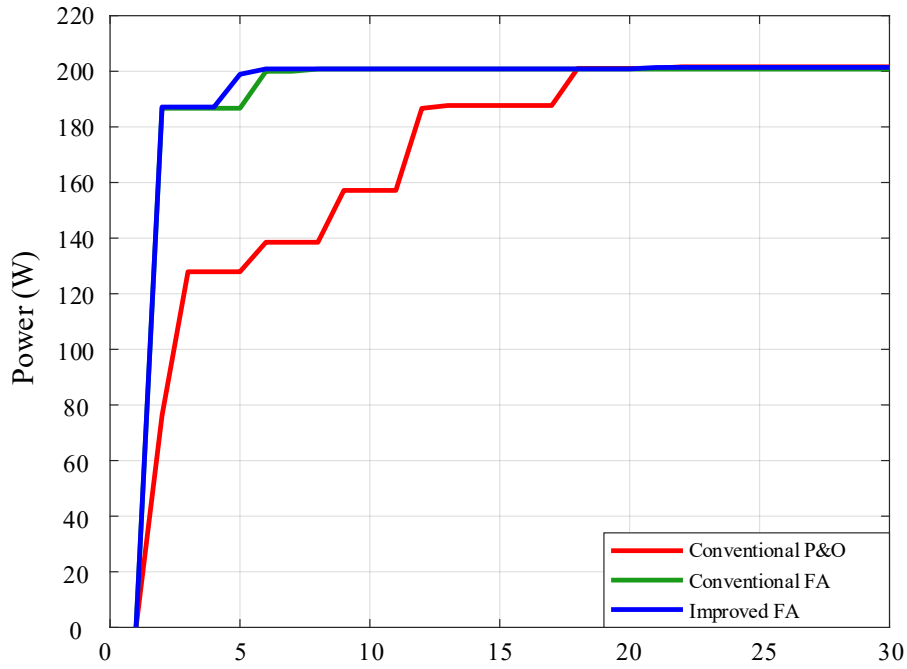

Figure 14. A tracking performance comparison between algorithms in Scenario 2.

(3) Scenario 3

In this scenario, 50% of a PV module and 70% of another were shaded, and three peaks occurred on the P-V curve, as illustrated in Figure 15. The maximum power was further reduced to 184.7 W, and there was one more peak on the P-V curve than in Scenario 2. The GMPP lay near the right endpoint of the curve again. The tracking performance is compared in Figure 16. As it appears, this work outperformed others again. After getting trapped in a LMPP, it took the improved version of the FA a shorter period of time to get away from the trap than the original version. Here, it must be stressed that the conventional P&O method failed to track down the GMPP even after 30 iterations.

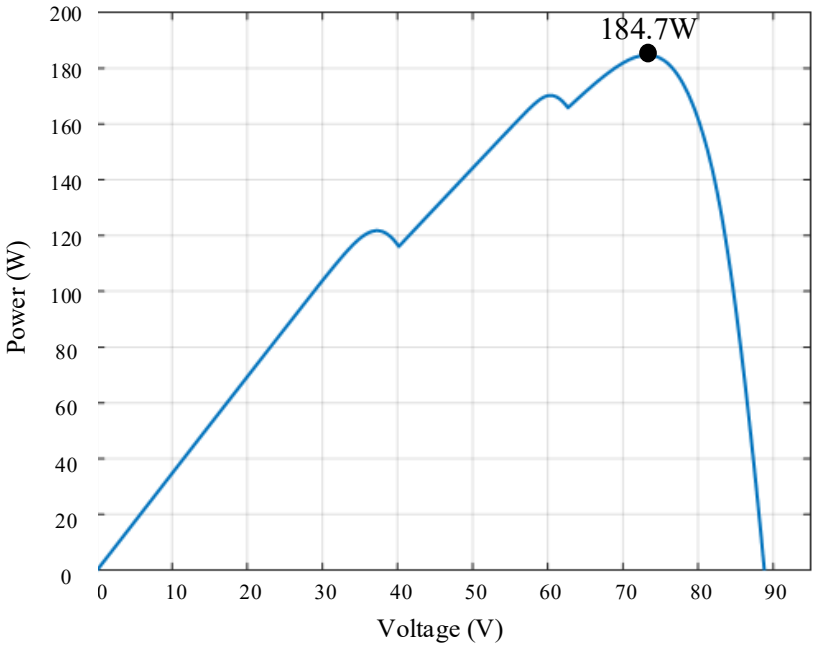

Figure 15. The P-V curve in Scenario 3.

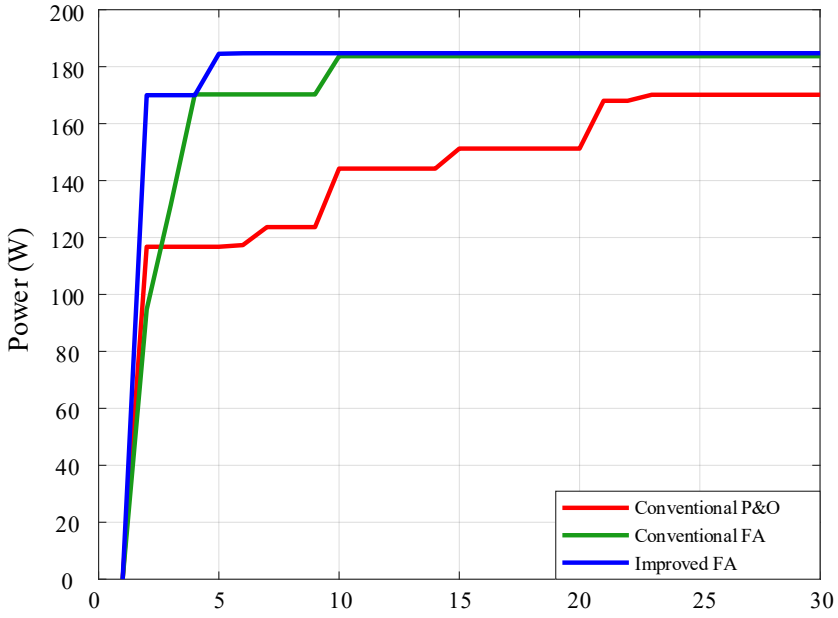

Figure 16. A tracking performance comparison between algorithms in Scenario 3.

(4) Scenario 4

In this scenario, 70% of a module was shaded in addition to the two shaded modules in Scenario 3. As illustrated in Figure 17, the maximum output power was further reduced to 184.7 W, and there was one more peak on the P-V curve than in Scenario 3. The GMPP lay near the right endpoint of the curve again. As can be seen in Figure 18, both the improved and the original version of the FA succeeded in tracking down the GMPP as expected, while the P&O method failed again. As before, this work outperformed the original version of the FA.

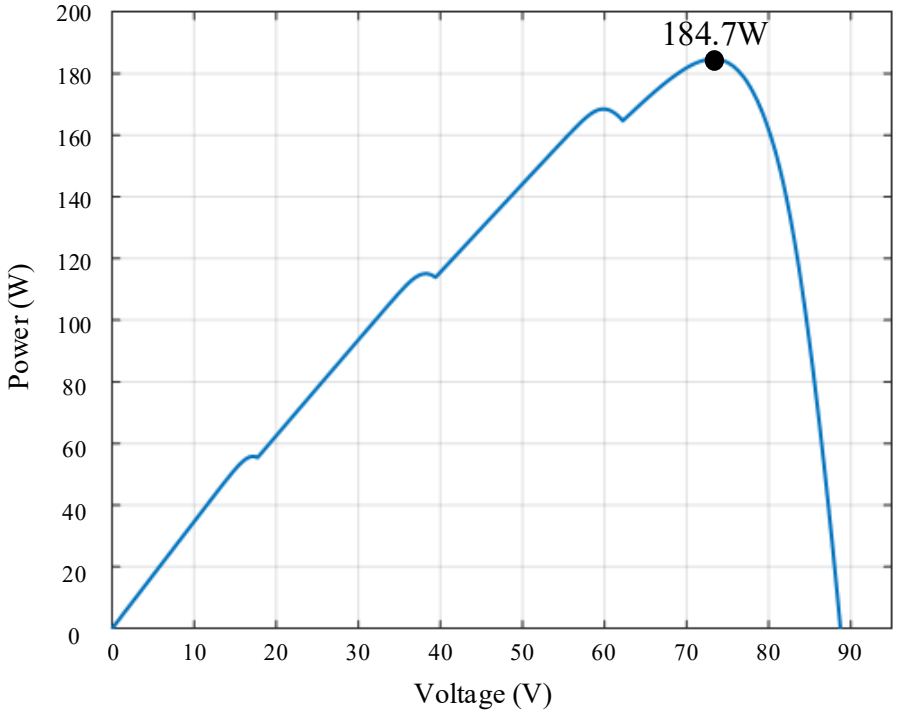

Figure 17. The P-V curve in Scenario 4.

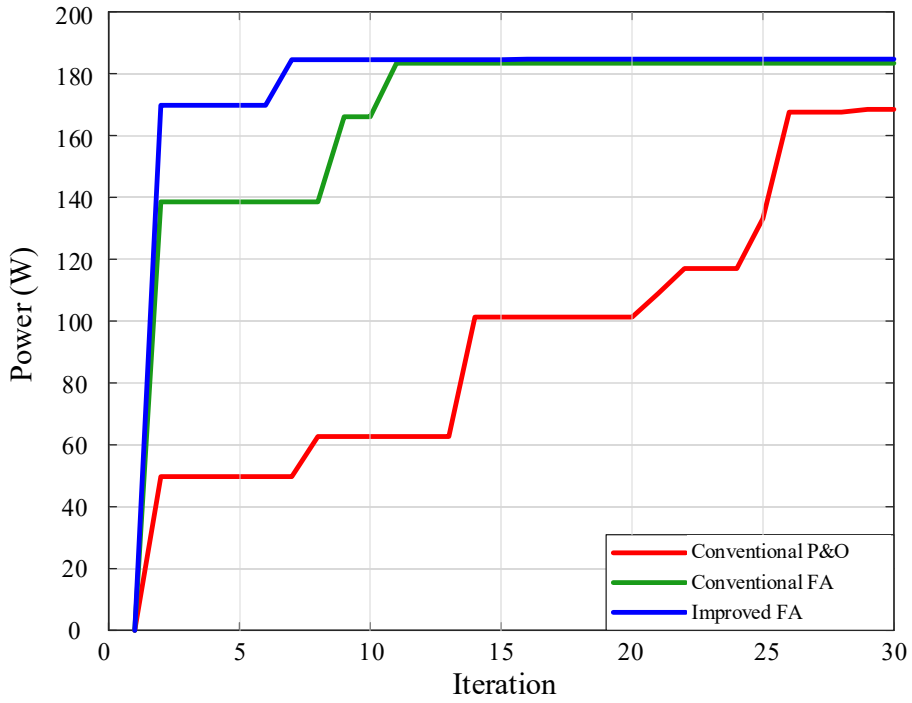

Figure 18. A tracking performance comparison between algorithms in Scenario 4.

(5) Scenario 5

As listed in Table 6, nine modules were shaded in this scenario, that is, 70% of the first third, 80% of the second third and 90% of the last third modules were shaded. As illustrated in Figure 19, there were 4 peaks on the P-V curve, and the global maximum output power was as low as 55.8 W. Unlike in Scenarios 1–4, the GMPP instead lay near the left endpoint of the P-V curve this time. In Figure 20, it is observed that the P&O method got trapped in a LMPP more easily than others, even though all the three algorithms finally succeeded in tracking down the GMPP. Above all, this work outperformed others again.

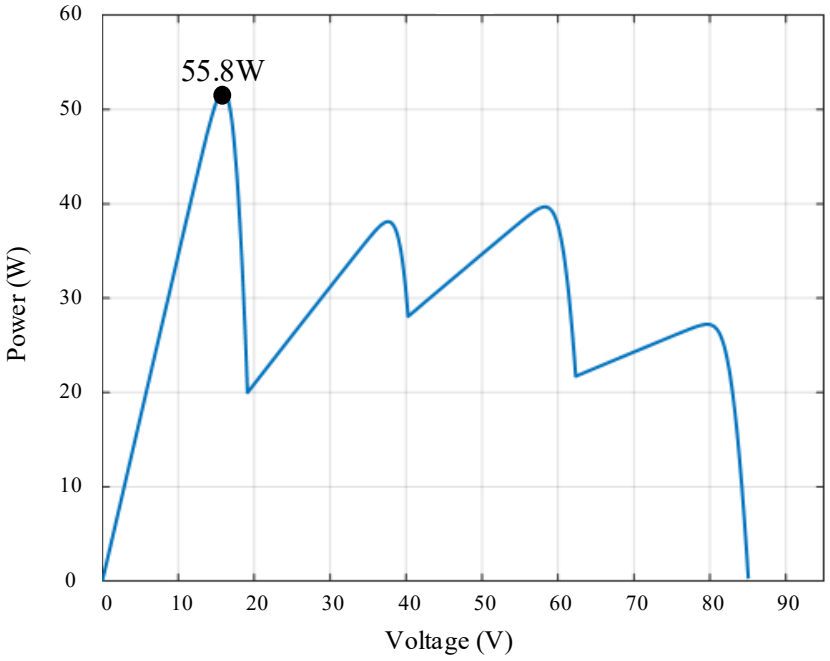

Figure 19. The P-V curve in Scenario 5.

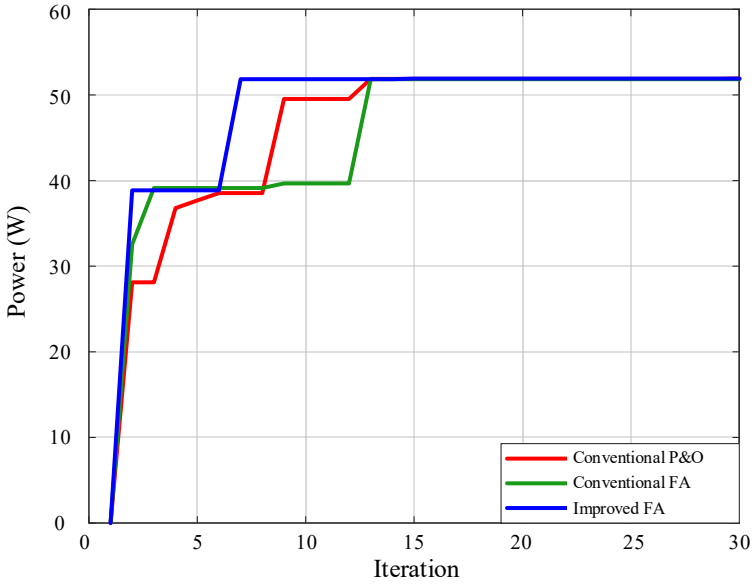

Figure 20. A tracking performance comparison between algorithms in Scenario 5.

5.3. Discussion of the Simulation Results

For readers' convenience, a tracking performance comparison in Scenarios 1–5 is listed in Table 7. The tracking performance was measured as the average number of iterations and the average tracking time required to track down the GMPP in 10 trials. Obviously, this work outperformed its counterparts, which highlights the robustness of this work against various shading conditions.

Table 7. A comparison of the average number of iterations and tracking time required to track down the GMPP in 10 trials.

Scenario	No. of Peaks on Respective P-V Curve	Average Number of Iterations/Average Tracking Time		
		Conventional P&O	Conventional FA	Improved FA
1	Single	10.4/5.2 s	5.6/2.8 s	3.4/0.7 s
2	Double (MPP was on the right peak)	19.5/7.6 s	8.4/3.4 s	5.7/0.9 s
3	Triple (MPP was on the rightmost peak)	not available	14.1/4.0 s	12.7/1.3 s
4	Quadruple (MPP was on the rightmost peak)	not available	14.3/4.2 s	12.8/1.6 s
5	Quadruple (MPP was on the leftmost peak)	22.8/5.8 s	17.2/4.7 s	14.1/2.0 s

At present, four test cases have been selected to conduct tracking performance tests for the number of peaks and the different locations of the peaks in different P-V characteristic curves generated under different shading conditions; they are compared with the conventional perturbation and observation (P&O) [3], the conventional grey wolf optimization (GWO) [18] and the conventional artificial bee colony (ABC) [24] algorithms, respectively, for tracking performance, the test results of which are summarized in Table 8.

Table 8. Comparison of simulation test results for four scenarios with different MPPT methods.

Scenario	No. Peak(s) of the P-V Curve	Method Proposed in [3]	Method Proposed in [18]	Method Proposed in [24]	Proposed in this Study
		Average Tracking Time	Average Tracking Time	Average Tracking Time	Average Tracking Time
1	Single-peak	10.4 s	8.6 s	8.58 s	3.4 s
2	Double-peak	19.5 s	12.5 s	20.01 s	5.7 s
3	Triple-peak	None *	15.4 s	31.3 s	12.7 s
4	Quadruple-peak	None *	20.8 s	24.21 s	12.8 s

Note: The symbol "None *" indicates that this reference does not provide the test results of this scenario.

Take Scenario 2 from the simulation results of the maximum power tracking conducted by the conventional P&O algorithm, the conventional FA and the improved FA in Figure 21 as an example; if the area of the region (such as the interval with black dotted lines) from the start point of tracking to the global maximum power point tracked by all methods acts as the optimal output energy of the PVMA in the tracking process, and the area of the region between the tracking curve for various methods to the tracked global maximum power point acts as its actual output energy, followed by calculating its tracking efficiency from the ratio of both areas, then the tracking efficiencies of five scenarios using different methods can be listed in Table 9 for comparison. It can be seen from Table 9 that, in different scenarios, the tracking efficiencies of the improved firefly optimization algorithm are the most optimal compared to the other methods, and all of them are above 89.76%. Whereas, in Scenarios 3 and 4, the conventional P&O achieves tracking efficiencies of as low as 67.88–42.48% within 30 iterations because the global maximum power point cannot be tracked.

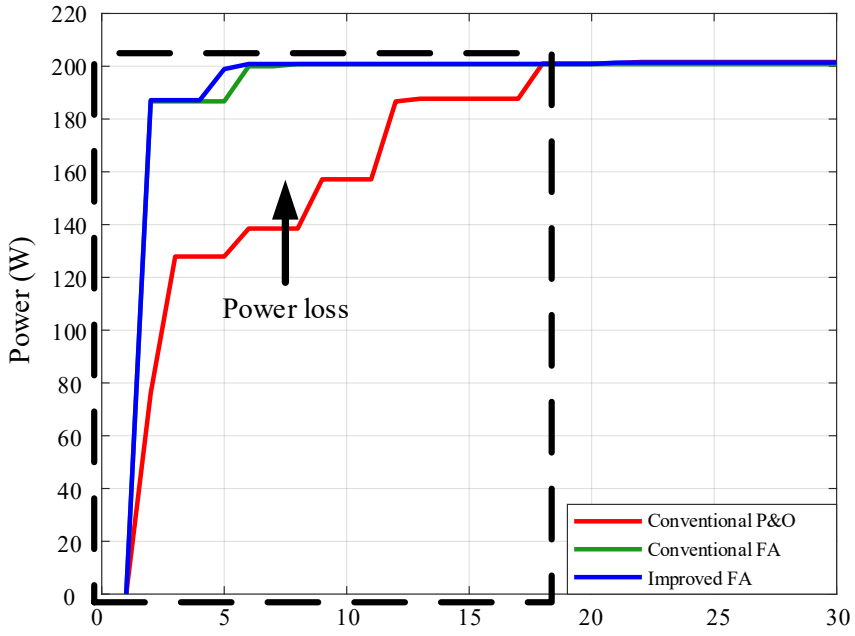

Figure 21. MPPT efficiency diagram of Scenario 2 obtained using the conventional P&O algorithm, conventional FA and improved FA.

Table 6 shows five test cases of the PVMA in 4 series-3 parallel form used under different shading conditions herein, in which all P-V characteristic curves of the PVMA are obtained from the simulation under standard test conditions (STC). Although the changes in both temperature and sunshine would affect its maximum power output, the impact on

the MPPT tracking process is not significant because of its little variation in the shape of the P-V characteristic curve.

Table 9. A tracking efficiency comparison of the five scenarios.

Scenario	No. of Peaks on Respective P-V Curve	Tracking Efficiency (%)		
		Conventional P&O	Conventional FA	Improved FA
1	Single	78.83%	98.32%	99.29%
2	Double (MPP was on the right peak)	79.25%	98.73%	99.09%
3	Triple (MPP was on the rightmost peak)	67.88%	93.23%	98.01%
4	Quadruple (MPP was on the rightmost peak)	42.48%	82.96%	96.74%
5	Quadruple (MPP was on the leftmost peak)	77.99%	76.1%	89.76%

In this paper, the maximum power tracking test has been conducted under five different shading conditions for the PVMA, and each of the shading conditions is equivalent to the change in the temperature and sunshine parameter so that it is identical to the robustness test of maximum power tracking (MPPT) under the consideration of parameter uncertainty in [43,44]. Moreover, from the test results in Tables 7–9, the proposed improved FA MPPT method has better performance in tracking speed and efficiency than other methods for the location of the global maximum power point (GMPP) in different cases, so that it is evident that the proposed MPPT method is indeed robust.

6. Conclusions

This work presents an improved version of the FA which happened to outperform the original version in terms of the GMPP tracking performance. Moreover, a high-voltage step-up converter was designed to raise an input voltage of 80 V to an output voltage of 400 V. This was done simply because the converter worked at a relatively low duty cycle, and the conversion efficiency was raised accordingly. Unlike in the original version of the FA, the step size was made adaptive to the slope of a P-V curve and the number of iterations. As a consequence, once having gotten trapped in a LMPP, the presented MPP tracker can easily escape from the trap and then succeed in tracking down the GMPP expeditiously as intended. The performance of the proposed MPP tracker was tested in five scenarios, and it has, accordingly, been validated as robust against various shading conditions. Subsequently, the TMS320F2809 digital signal processor (DSP) produced by Texas Instruments will be used as the control core for implementation in the future to ensure the effectiveness and robustness of the proposed method.

Author Contributions: K.-H.C. planned, wrote, edited and reviewed the project. S.-W.Z. was responsible for using the Matlab software to simulate photovoltaic module arrays for maximum power point tracking and the PSIM software to simulate the high-voltage step-up converter. K.-H.C. managed the project. All authors have read and agreed to the published version of the manuscript.

Funding: The authors gratefully acknowledge the support and funding of this project by the Ministry of Science and Technology, Taiwan, under the Grant Number MOST 110-2221-E-167-067-MY2.

Institutional Review Board Statement: Not applicable.

Informed Consent Statement: Not applicable.

Data Availability Statement: This study did not report any data.

Conflicts of Interest: The authors of the manuscript declare no conflict of interest.

References

1. Wei, Q.; Shi, G.; Song, R.; Liu, Y. Adaptive Dynamic Programming-based Optimal Control Scheme for Energy Storage Systems with Solar Renewable Energy. *IEEE Trans. Ind. Electron.* **2017**, *64*, 5468–5478. [CrossRef]
2. Safdarian, A.; Fotuhi-Firuzabad, M.; Aminifar, F. Compromising Wind and Solar Energies from the Power System Adequacy Viewpoint. *IEEE Trans. Power Syst.* **2012**, *27*, 2368–2376. [CrossRef]
3. Jones, D.C.; Erickson, R.W. Probabilistic Analysis of a Generalized Perturb and Observe Algorithm Featuring Robust Operation in the Presence of Power Curve Traps. *IEEE Trans. Power Electron.* **2013**, *28*, 2912–2926. [CrossRef]
4. Killi, M.; Samanta, S. Modified Perturb and Observe MPPT Algorithm for Drift Avoidance in Photovoltaic Systems. *IEEE Trans. Ind. Electron.* **2015**, *62*, 5549–5559. [CrossRef]
5. Sher, H.A.; Murtaza, A.F.; Noman, A.; Addoweesh, K.E.; Al-Haddad, K.; Chiaberge, M. A New Sensorless Hybrid MPPT Algorithm Based on Fractional Short-circuit Current Measurement and P&O MPPT. *IEEE Trans. Sust. Energy* **2015**, *6*, 1426–1434.
6. Sahu, R.K.; Ghosh, A. Maximum Power Generation from Solar Panel by Using P&O MPPT. In Proceedings of the International Conference on Intelligent Controller and Computing for Smart Power (ICICCSP), Hyderabad, India, 21–23 July 2022; pp. 1–4.
7. Utaikaifa, K. Reduction of Power Ripple in P&O MPPT System Using Output Feedback. In Proceedings of the 4th International Conference on Power Engineering, Energy and Electrical Drives, Istanbul, Turkey, 13–17 May 2013; pp. 427–432.
8. Szemes, P.T.; Melhem, M. Analyzing and Modeling PV with "P&O" MPPT Algorithm by MATLAB/SIMULINK. In Proceedings of the 3rd International Symposium on Small-Scale Intelligent Manufacturing Systems (SIMS), Gjovik, Norway, 10–12 June 2020; pp. 1–6.
9. Liu, F.; Duan, S.; Liu, F.; Liu, B.; Kang, Y. A Variable Step Size INC MPPT Method for PV Systems. *IEEE Trans. Ind. Electron.* **2008**, *55*, 2622–2628.
10. Bhattacharyya, S.; Kumar, D.S.; Samanta, S.; Mishra, S. Steady Output and Fast Tracking MPPT (SOFT-MPPT) for P&O and INC Algorithms. *IEEE Trans. Sust. Energy* **2021**, *12*, 293–302.
11. Saber, H.; Bendaouad, A.E.; Rahmani, L.; Radjeai, H. A Comparative Study of the FLC, INC and P&O Methods of the MPPT Algorithm for a PV System. In Proceedings of the 19th International Multi-Conference on Systems, Signals & Devices (SSD), Sétif, Algeria, 6–10 May 2022; pp. 2010–2015.
12. Zhang, H.; Li, S.Z.; Zhang, X.N.; Xia, Y.L. MPPT Control Strategy for Photovoltaic Cells Based on Fuzzy Control. In Proceedings of the 12th International Conference on Natural Computation, Fuzzy Systems and Knowledge Discovery (ICNC-FSKD), Changsha, China, 13–15 August 2016; pp. 450–454.
13. Subasic, P.; Nakatsuyama, M. A New Representational Framework for Fuzzy Sets. In Proceedings of the 6th International Fuzzy Systems Conference, Barcelona, Spain, 5 July 1997; pp. 1601–1606.
14. Rai, R.K.; Rahi, O.P. Fuzzy Logic based Control Technique Using MPPT for Solar PV System. In Proceedings of the First International Conference on Electrical, Electronics, Information and Communication Technologies (ICEEICT), Trichy, India, 16–18 February 2022; pp. 1–5.
15. Prokhorov, D. Echo State Networks: Appeal and Challenges. In Proceedings of the IEEE International Joint Conference on Neural Networks, Montreal, QC, Canada, 31 July–4 August 2005; pp. 1463–1466.
16. Dahidi, S.A.; Ayadi, O.; Alrbai, M.; Adeeb, J. Ensemble Approach of Optimized Artificial Neural Networks for Solar Photovoltaic Power Prediction. *IEEE Access* **2019**, *7*, 81741–81758. [CrossRef]
17. Shukla, A.; Titare, L.S. An Efficient Neural Network-based MPPT Technique for PV Array under Partial Shading Conditions. In Proceedings of the International Conference on Smart Generation Computing, Communication and Networking (SMART GENCON), Pune, India, 29–30 October 2021; pp. 1–5.
18. Mohanty, S.; Subudhi, B.; Ray, P.K. A Grey Wolf Optimization Based MPPT for PV System under Changing Insolation Level. In Proceedings of the IEEE Students' Technology Symposium (TechSym), Kharagpur, India, 30 September–2 October 2016; pp. 175–179.
19. Atici, K.; Sefa, I.; Altin, N. Grey Wolf Optimization Based MPPT Algorithm for Solar PV System with SEPIC Converter. In Proceedings of the 4th International Conference on Power Electronics and their Applications (ICPEA), Elazig, Turkey, 25–27 September 2019; pp. 1–6.
20. Hasan, F.R.; Prasetyono, E.; Sunarno, E. A Modified Maximum Power Point Tracking Algorithm Using Grey Wolf Optimization for Constant Power Generation of Photovoltaic System. In Proceedings of the International Conference on Artificial Intelligence and Mechatronics Systems (AIMS), Bandung, Indonesia, 28–30 April 2021; pp. 1–6.
21. Firmanza, A.P.; Habibi, M.N.; Windarko, N.A.; Yanaratri, D.S. Differential Evolution-based MPPT with Dual Mutation for PV Array under Partial Shading Condition. In Proceedings of the 10th Electrical Power, Electronics, Communications, Controls and Informatics Seminar (EECCIS), Malang, Indonesia, 26–28 August 2020; pp. 198–203.
22. Tajuddin, M.F.N.; Ayob, S.M.; Salam, Z. Tracking of Maximum Power Point in Partial Shading Condition Using Differential Evolution (DE). In Proceedings of the IEEE International Conference on Power and Energy (PECon), Kota Kinabalu, Malaysia, 2–5 December 2012; pp. 384–389.

23. Taheri, H.; Salam, Z.; Ishaque, K. Syafaruddin A Novel Maximum Power Point Tracking Control of Photovoltaic System under Partial and Rapidly Fluctuating Shadow Conditions Using Differential Evolution. In Proceedings of the IEEE Symposium on Industrial Electronics and Applications (ISIEA), Penang, Malaysia, 3–5 October 2010; pp. 82–87.
24. Castano, C.G.; Restrepo, C.; Kouro, S.; Rodriguez, J. MPPT Algorithm Based on Artificial Bee Colony for PV System. *IEEE Access* **2021**, *9*, 43121–43133. [CrossRef]
25. Li, N.; Mingxuan, M.; Yihao, W.; Lichuang, C.; Lin, Z.; Qianjin, Z. Maximum Power Point Tracking Control Based on Modified ABC Algorithm for Shaded PV System. In Proceedings of the International Conference of Electrical and Electronic Technologies for Automotive (AEIT AUTOMOTIVE), Turin, Italy, 2–4 July 2019; pp. 1–5.
26. Pilakkat, D.; Kanthalakshmi, S. Artificial Bee Colony Algorithm for Peak Power Point Tracking of a Photovoltaic System under Partial Shading Condition. In Proceedings of the International Conference on Current Trends towards Converging Technologies (ICCTCT), Coimbatore, India, 1–3 March 2018; pp. 1–7.
27. Huang, Y.P.; Huang, M.Y.; Ye, C.E. A Fusion Firefly Algorithm with Simplified Propagation for Photovoltaic MPPT under Partial Shading Conditions. *IEEE Trans. Sust. Energy* **2020**, *11*, 2641–2652. [CrossRef]
28. Teshome, D.F.; Lee, C.H.; Lin, Y.W.; Lian, K.L. A Modified Firefly Algorithm for Photovoltaic Maximum Power Point Tracking Control under Partial Shading. *IEEE J. Emerg. Sel. Topics Power Electron.* **2016**, *5*, 661–671. [CrossRef]
29. Windarko, N.A.; Tjahjono, A.; Anggriawan, D.O.; Purnomo, M.H. Maximum Power Point Tracking of Photovoltaic System Using Adaptive Modified Firefly Algorithm. In Proceedings of the International Electronics Symposium (IES), Surabaya, Indonesia, 29–30 September 2015; pp. 31–35.
30. Li, C.C.; Sun, C.Y.; Li, S.Q.; Zhang, Y.Y. An Integrated MPPT Control Strategy Using Circle Search-firefly Algorithm (CSFA) for Photovoltaic System. In Proceedings of the 4th International Conference on Smart Power & Internet Energy Systems (SPIES), Beijing, China, 9–12 December 2022; pp. 1945–1949.
31. Mohammad, M.; Rabeh, A.; Houssem, J.; Faraedoon, W.A.; Halkawt, A.; Alireza, R. A New MPPT Design Using Variable Step Size Perturb and Observe Method for PV System under Partially Shaded Conditions by Modified Shuffled Frog Leaping Algorithm-SMC Controller. *Sustain. Energy Technol. Assess.* **2021**, *45*, 101056.
32. Guo, S.; Abbassi, R.; Jerbi, H.; Rezvani, A.; Suzuki, K. Efficient Maximum Power Point Tracking for a Photovoltaic Using Hybrid Shuffled Frog-leaping and Pattern Search Algorithm under Changing Environmental Conditions. *J. Clean. Prod.* **2021**, *297*, 126573. [CrossRef]
33. Tian, H.; Bai, Q.; Li, X.; Han, H.; Maoa, S.; Yang, H.; Wang, H. Comparative Study on Fill Factor of PERC Silicon Solar Cells and Al-BSF Silicon Solar Cells under Non-standard Test Conditions. In Proceedings of the IEEE 48th Photovoltaic Specialists Conference (PVSC)s, Fort Lauderdale, FL, USA, 20–25 June 2021; pp. 256–259.
34. Forouzesh, M.; Siwakoti, Y.P.; Gorji, S.A.; Blaabjerg, F.; Lehman, B. Step-up DC–DC Converters: A Comprehensive Review of Voltage-boosting Techniques, Topologies, and Applications. *IEEE Trans. Power Electron.* **2017**, *32*, 9143–9178. [CrossRef]
35. Park, D.; Lee, H. Improvements in Light-load Efficiency and Operation Frequency for Low-voltage Current-mode Integrated Boost Converters. *IEEE Trans. Circuits Syst. II Express Briefs* **2014**, *61*, 599–603. [CrossRef]
36. Park, K.B.; Moon, G.W.; Youn, M.J. Overview of High-step-up Coupled-inductor Boost Converters. *IEEE J. Emerg. Sel. Topics Power Electron.* **2016**, *4*, 689–704.
37. Park, K.B.; Moon, G.W.; Youn, M.J. Nonisolated High Step-up Stacked Converter Based on Boost-integrated Isolated Converter. *IEEE Trans. Power Electron.* **2011**, *26*, 577–587. [CrossRef]
38. Schmitz, L.; Martins, D.C.; Coelho, R.F. Generalized High Step-up DC-DC Boost-based Converter with Gain Cell. *IEEE Trans. Circuits Syst. I: Regular Papers* **2017**, *64*, 480–493. [CrossRef]
39. Park, K.B.; Moon, G.W.; Youn, M.J. Nonisolated High Step-up Boost Converter Integrated with Sepic Converter. *IEEE Trans. Power Electron.* **2010**, *25*, 2266–2275. [CrossRef]
40. Park, K.B.; Moon, G.W.; Youn, M.J. High Step-up Boost Converter Integrated with a Transformer-assisted Auxiliary Circuit Employing Quasi-resonant Operation. *IEEE Trans. Power Electron.* **2012**, *27*, 1974–1984. [CrossRef]
41. PSIM-User-Manual.pdf, Powersim. Available online: https://powersimtech.com/wp-content/uploads/2021/01/PSIM-User-Manual.pdf (accessed on 21 February 2023).
42. Chao, K.H.; Zhang, S.W. An Maximum Power Point Tracker of Photovoltaic Module Arrays Based on Improved Firefly Algorithm. *Sustainability* **2023**, *15*, 8550. [CrossRef]
43. Khan, R.; Khan, L.; Ullah, S.; Sami, I.; Ro, J.S. Backstepping Based Super-Twisting Sliding Mode MPPT Control with Differential Flatness Oriented Observer Design for Photovoltaic System. *J. Power Electron.* **2020**, *9*, 1543. [CrossRef]
44. Ali, K.; Khan, L.; Khan, Q.; Ullah, S.; Ahmad, S.; Mumtaz, S.; Karam, F.W.; Naghmash. Robust Integral Backstepping Based Nonlinear MPPT Control for a PV System. *Energies* **2019**, *12*, 3180. [CrossRef]